

# Quantum Phase Transition, $O(3)$ Universality Class and Phase Diagram of Spin-1/2 Heisenberg Antiferromagnet on Distorted Honeycomb Lattice: A Tensor Renormalization Group Study

Wei Li, Shou-Shu Gong, Yang Zhao, and Gang Su\*

College of Physical Sciences, Graduate University of Chinese Academy of Sciences, P. O. Box 4588, Beijing 100049, China

The spin-1/2 Heisenberg antiferromagnet on the distorted honeycomb (DHC) lattice is studied by means of the tensor renormalization group method. It is unveiled that the system has a quantum phase transition of second-order between the gapped quantum dimer phase and a collinear Néel phase at the critical point of coupling ratio  $\alpha_c \simeq 0.54$ , where the quantum critical exponents  $\nu \simeq 0.69(2)$  and  $\gamma \simeq 1.363(8)$  are obtained. The quantum criticality is found to fall into the  $O(3)$  universality class. A ground-state phase diagram in the field-coupling ratio plane is proposed, where the phases such as the dimer, semi-classical Néel, and polarized phases are identified. A link between the present spin system to the boson Hubbard model on the DHC lattice is also discussed.

PACS numbers: 75.10.Jm, 75.40.Mg, 64.70.Tg, 05.30.Jp

## I. INTRODUCTION

Since the discovery of high temperature superconductors, the two-dimensional (2D) Heisenberg models have received particular attention in the past decades. Several numerical works show that the spin-1/2 isotropic Heisenberg antiferromagnet (HAF) on a square lattice exhibits an AF long-range order (LRO) in the ground state<sup>2,3</sup>, although a mathematically rigorous proof still lacks now. Various methods (e.g. the spin wave analysis<sup>4</sup>, different numerical techniques<sup>5</sup>, etc.) were also applied to investigate the properties of this model. When the bond anisotropy is introduced, the magnetic order-disorder quantum phase transition (QPT) can be identified<sup>6-10</sup>. Another intriguing 2D bipartite lattice—the honeycomb (HC) lattice has also been studied with various methods, such as quantum Monte Carlo (QMC)<sup>2</sup>, series expansion<sup>11</sup>, spin wave<sup>12</sup> and newly proposed tensor renormalization group (TRG) method<sup>13</sup>. These investigations show that owing to the lowest coordinates among 2D lattices, the system is more affected by quantum fluctuations, giving rise to the spontaneous magnetization per site of the spin-1/2 HAF model on this lattice smaller than that on a square lattice.

Recently, people have obtained a number of magnetic materials with distorted honeycomb (DHC) lattices, such as  $\text{MnPS}_3$  and  $\text{FePS}_3$ <sup>14</sup>,  $\text{Cu}_{2/3}\text{V}_{1/3}\text{O}_3$ <sup>15</sup>,  $\text{Na}_3\text{Cu}_2\text{SbO}_6$ <sup>16</sup>, and  $\text{Mn}[\text{C}_{10}\text{H}_6(\text{OH})(\text{COO})]_2 \times 2\text{H}_2\text{O}$ <sup>17</sup>, where the magnetic ions (e.g.  $\text{Cu}^{+2}$  and  $\text{Mn}^{+2}$ ) form an HC lattice with different nearest-neighbor (NN) bonds. The magnetic properties of these materials have been investigated experimentally. However, the theoretical studies on the HAF model on the DHC lattice are still sparse. There is a recent work that explores the ground state properties of the Heisenberg model on a DHC lattice by QMC calculations<sup>18</sup>, and the order-disorder QPT in zero magnetic field has been observed. Nevertheless, the magnetic properties of the model on such a DHC lattice in nonzero external fields are not yet seen in literature. Therefore, in order to understand the experimental observations profoundly, it should pay more theoretical attention on the HAF model on the DHC lattice.

In this paper, by means of the newly developed TRG method and a variational analysis, we shall study the ground

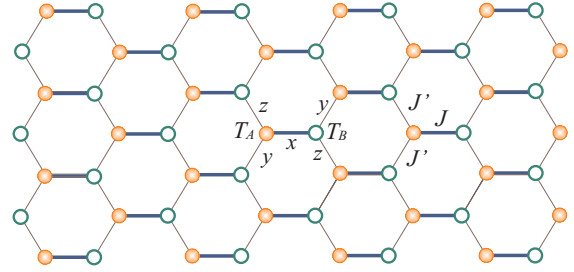


FIG. 1: (Color online) The distorted honeycomb lattice can be viewed as a tensor network, where  $T_A$  ( $T_B$ ) are the tensors located on A (B) sublattice (indicated by different symbols), and each tensor has three bond indices labeled by  $x$ ,  $y$ , and  $z$ .

state properties of the spin-1/2 HAF model on the DHC lattice with and without magnetic fields. On one hand, our primary purpose is to understand the ground state properties of the model under consideration in the presence of a magnetic field, and on the other hand, we also want to test the accuracy of TRG methods in a more extensive range rather than a spatially bond isotropic case by comparing our calculated results with the previous studies on HC and DHC lattices using other methods. Owing to the limitation of the present TRG scheme, a finite-temperature calculation on the Heisenberg model is still not feasible now, which makes it impossible to compare directly the calculated results with the experiments. Our study shows that the spin-1/2 Heisenberg model on a DHC lattice has a second-order QPT with respect to the bond coupling ratio, that is determined to fall into the  $O(3)$  universality class by identifying the two quantum critical exponents. A phase diagram separating the dimer, polarized, canted Néel and Néel phases is also proposed. The magnetic properties in the presence of a magnetic field are obtained, where some interesting behaviors are observed. In addition, the TRG method has been verified through this present model to give a good agreement with most of the previous studies, but it might overestimate slightly the spontaneous sublattice magnetization per site on the HC lattice, implying that the TRG method may still need more works for improvements.

The other parts of this paper is organized as follows. In Sec.

II, the model Hamiltonian and the TRG method will be introduced. In Sec. III, the magnetic properties of the model under interest in the absence of a magnetic field will be reexamined with the TRG algorithm. In Sec. IV, the ground state properties in the presence of a magnetic field will be explored, and a phase diagram will be proposed. In Sec. V, by invoking a boson mapping, the present model is mapped onto the 2D boson Hubbard model, whose properties will be briefly discussed. Finally, a conclusion will be given.

## II. MODEL HAMILTONIAN AND NUMERICAL METHOD

The system under interest is schematically depicted in Fig. 1. The Hamiltonian reads

$$H = J \sum_{\langle i,j \rangle_x} \mathbf{S}_i \cdot \mathbf{S}_j + J' \sum_{\langle i,j \rangle_{yz}} \mathbf{S}_i \cdot \mathbf{S}_j - h \sum_i S_i^z - h_s \sum_i \epsilon_i S_i^z, \quad (1)$$

where  $\mathbf{S}_i$  denotes the spin-1/2 operator at site  $i$ ,  $\langle i,j \rangle_x$  labels the NN spins along the rungs ( $x$  bond),  $\langle i,j \rangle_{yz}$  means the NN spins along the zigzag directions ( $y$  and  $z$  bonds),  $J$  is the interaction on the  $x$  bond,  $J'$  is the interaction on the  $y$  or  $z$  bond,  $h$  and  $h_s$  stand for the uniform and staggered magnetic fields, respectively, and  $\epsilon_i = +1$  when  $i$  on  $A$  sublattice and  $-1$  on  $B$  sublattice. We introduce for convenience a bond coupling ratio  $\alpha = J'/J$ , and take  $J$  as an energy scale.

To explore the ground state properties of the present system we shall utilize the TRG method. This numerical algorithm was first introduced to calculate the thermodynamic properties of the 2D classical models<sup>19</sup>, and then generalized to obtain the expectation values of observables in the quantum state with the tensor product wave functions (e.g. Ref.13) on bipartite lattices given by

$$|\Psi\rangle = \sum_{\{x_i, y_i, z_i=1\}}^D \prod_{i \in A, j \in B} (T_A)_{x_i, y_i, z_i}^{m_i} (T_B)_{x_j, y_j, z_j}^{m_j} |m_i m_j\rangle, \quad (2)$$

where  $T_A$  ( $T_B$ ) represents the tensor located on  $A$  ( $B$ ) sublattice, over which the indices  $i$  and  $j$  run, and the summation over all bond indices  $x, y, z$  is from 1 to the bond dimension  $D$ . According to the TRG algorithm, the ground state wave function and energy can be directly obtained by using trial wave functions of tensor product form<sup>20</sup>. This variational scheme, however, is not so efficient that makes the achievable bond dimension  $D$  not larger than 3 in general due to huge variational parameter space. Recently, it was improved by combining the infinite time-evolving block decimation (iTEBD)<sup>21</sup> and TRG method to determine the ground state and to get the expectation values of local observables<sup>13</sup>. This alternative algorithm appears to be accurate and efficient, in which the available bond dimension  $D$  can reach as large as 8, and the calculated results agree well with those obtained by other methods. It has been applied to study the spin flop transition of spin-1/2  $XXZ$  model on a square lattice<sup>22</sup>. In the following, we shall adopt this novel scheme to calculate the physical quantities of the spin-1/2 HAF system on the DHC lattice.

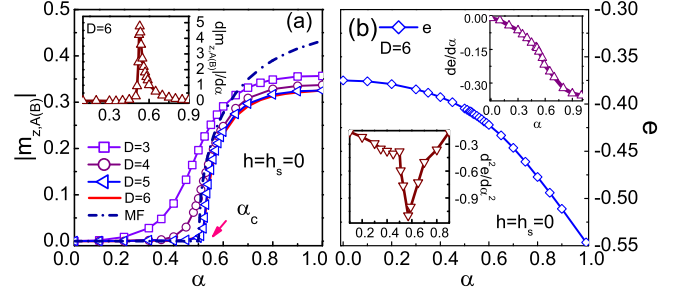


FIG. 2: (Color online) (a) The spontaneous sublattice magnetization per site  $|m_{z,A(B)}|$  as a function of the bond ratio  $\alpha$  for different bond dimensions  $D = 3, 4, 5, 6$ . The dashed dot line represents the mean-field result [Eq. (5)]. The inset gives the derivative of  $|m_{z,A(B)}|$  as a function of  $\alpha$ , where a discontinuity at  $\alpha_c \simeq 0.54$  is observed. (b) The ground state energy per site  $e$  and its derivatives (insets: first- and second-order) versus  $\alpha$ , where the discontinuity in  $\partial^2 e / \partial \alpha^2$  against  $\alpha$  indicates a QPT of second-order.

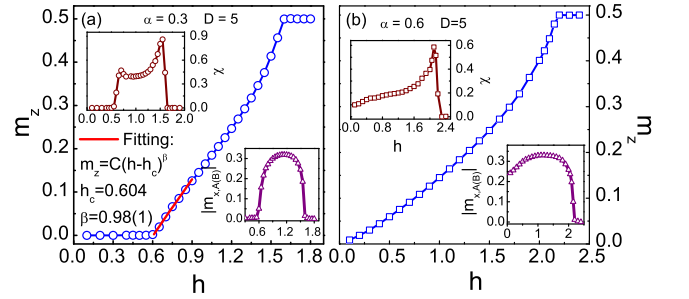


FIG. 3: (Color online) The magnetization per site as a function of magnetic field  $h$ . The insets show the susceptibility  $\chi$  (upper panel) and the transverse component of sublattice magnetization per site  $|m_{x,A(B)}|$  (lower panel) as functions of  $h$ . (a)  $\alpha = 0.3$ ; (b)  $\alpha = 0.6$ , where  $D = 5$  and  $h_s = 0$  for both. The fitting curves in (a) shows a nearly linear behavior of  $m_z$ , with  $\beta \simeq 0.98(1)$ . The number in the parenthesis denotes numerical fitting error hereafter.

In our practical calculations, during the iterative projections by evolution operator ( $e^{-\tau H}$ ) along the imaginary time  $\tau$  axis, we first start with a step  $\delta\tau = 10^{-3}$ , and then diminish it gradually to  $\delta\tau = 10^{-5}$ . The total number of iterations is taken as about  $10^5 \sim 10^6$ , where  $D = 5$  or  $6$  is generally chosen. The convergence is always checked, as shown in Fig. 2(a) for different bond dimensions  $D$ .

## III. MAGNETIC ORDER-DISORDER TRANSITION

Let us first consider the case in absence of a magnetic field ( $h = 0$  and  $h_s = 0$ ). When  $\alpha = 0$ , the spins are coupled only by  $J$  along  $x$  bonds, and the ground state is  $|\Psi_g\rangle = \prod_{i \in A} \frac{1}{\sqrt{2}} [|\uparrow_i \downarrow_{i+x}\rangle - |\downarrow_i \uparrow_{i+x}\rangle]$  with energy  $-0.75J$

per bond, which is usually termed as a dimer state. This disordered ground state is protected by a finite spin singlet-triplet gap. When  $J'$  is set in, but  $\alpha$  is still small, one may conceive that the system may retain in the dimer phase<sup>6</sup>. This is confirmed in Fig. 2(a), where the spontaneous sublattice magnetization per site,  $m_{z,A(B)} = \frac{1}{N_{A(B)}} \sum_{i \in A(B)} \langle S_i^z \rangle$  with  $N_{A(B)}$  the total number of sublattice A(B) sites, as a function of  $\alpha$  is presented for  $D = 3, 4, 5, 6$ . It is seen that there exists a critical ratio  $\alpha_c$  below which  $m_{z,A(B)}$  vanishes, showing that the ground state for  $\alpha < \alpha_c$  is disordered and dominated by quantum fluctuations. For  $\alpha > \alpha_c$ , the ground state of the system has an AFLRO owing to a spontaneous  $SU(2)$  symmetry breaking. To determine the value of  $\alpha_c$  with accuracy, we have calculated the derivative of  $|m_{z,A(B)}|$  with respect to  $\alpha$  for  $D = 6$ , and found a discontinuity at  $\alpha = \alpha_c$ , where  $\alpha_c$  can be readily determined as 0.54.

To confirm if the transition occurring at  $\alpha_c$  is a QPT, we have also studied the ground state energy per site  $e$  as a function of  $\alpha$ . The results are presented in Fig. 2(b). It may be observed that with increasing  $\alpha$ , both  $e$  and its first derivative  $\partial e / \partial \alpha$  versus  $\alpha$  decrease continuously, but the second derivative  $\partial^2 e / \partial \alpha^2$  against  $\alpha$  shows a discontinuity at  $\alpha_c \simeq 0.54$ , as seen from the inset of Fig. 2(b). This feature characterizes a typical QPT of second-order.

It should be noted that, as shown in Fig. 2(a), we get  $|m_{z,A(B)}| \simeq 0.32$  ( $D = 6$ ) for  $\alpha = 1$ , which appears to overestimate the spontaneous sublattice magnetization per site on the HC lattice in comparison to the recent stochastic series expansion QMC result 0.2681(8) (Ref. 23), the "world line" QMC result 0.22 (Ref. 2), series expansion 0.27 (Ref. 11), and the spin-wave result 0.24 (Ref. 12). Such a discrepancy on  $m_{z,A(B)}$  has also been noted in Ref. 24, where they reported the sublattice magnetization per site on the HC lattice to be 0.3098 for  $D = 16$  by the TRG calculations. This slight discrepancy on the sublattice magnetization per site may come from the underestimation of quantum fluctuations in the absence of a magnetic field in the assumption of the tensor product state employed in the TRG method, because the isotropic system at  $\alpha = 1$  is gapless and has long-range correlations, where the quantum fluctuations may be strong. However, the ground state energy per site we obtained (-0.5465) for  $\alpha = 1$  ( $D = 6$ ) is quite consistent with those obtained for the HC lattice by other methods, e.g. the QMC result -0.5450 (Ref. 2), series expansion -0.5443 (Ref. 11), and the spin-wave result -0.5489 (Ref. 12). Therefore, as the critical point determined by the spontaneous sublattice magnetization [Fig. 2 (a)] coincides with that obtained from the singularity of the ground state energy [Fig. 2 (b)], it shows that the critical point is determined with rather assurance. In the presence of a magnetic field, since the quantum fluctuations are much suppressed, the results given by the TRG method should be reliable. This can also be validated in the following studies, including the attained linear behavior of the magnetization curves immediately above the critical magnetic field  $h_c$  [Fig. 3 (a)] and the verified relation  $H_{sat} = 2S(2\alpha + 1)$  of the saturation line that separates the canted Néel phase and polarized phase in Fig. 4, which is also consistent with that derived from the classical energy of spin wave analysis by a variational scheme<sup>4,17</sup>.

Another fact is that when the critical exponents of  $\nu$  and  $\gamma$  are determined (in Sec. IV), the critical point is approached from the dimer phase, and hence it is independent of the magnitude of spontaneous sublattice magnetization in the Néel phase. The obtained  $\nu$  and  $\gamma$  agree well with previous calculations and theoretical predictions, showing again that TRG method is fairly feasible for the present case.

In order to examine our numerical results, we perform a mean-field treatment in terms of a simple variational trial wave function

$$|\Psi_{var}\rangle = \prod_{i \in A} \frac{1}{\sqrt{1+t^2}} [|\uparrow_i \downarrow_{i+x}\rangle - t |\downarrow_i \uparrow_{i+x}\rangle], \quad (3)$$

that was applied to describe both disordered and ordered phases on a dimerized square lattice<sup>7</sup> and in a bilayer system<sup>25</sup>, where the lattice site  $i$  and  $i+x$  are NN sites along  $x$  bonds, and  $t$  is a variational parameter and interpolates between a singlet collection ( $t = 1$ ) and a classical Néel state ( $t = 0$ ). Substituting Eq. (1) (with  $h, h_s = 0$ ) and Eq. (3) into  $E_{var} = \langle \Psi_{var} | H | \Psi_{var} \rangle$  and minimizing it with respect to  $t$ , we obtain an upper bound for the ground state energy as

$$E_{var}/NJ = \begin{cases} -3/8, & \text{for } \alpha \leq 0.5 \\ -\frac{1}{16}(1/\alpha + 4\alpha + 2), & \text{for } \alpha > 0.5 \end{cases} \quad (4)$$

where  $N = N_A + N_B$  is the total number of lattice sites. Obviously,  $E_{var}$  is singular at  $\alpha_{c,var} = 0.5$ , showing  $\alpha_{c,var}$ , that is close to  $\alpha_c = 0.54$ , may be a transition point. The variational sublattice magnetization per site  $m_{var} = (1/N_A) \sum_{i \in A} \langle \Psi_{var} | S_i^z | \Psi_{var} \rangle$  can be obtained by

$$m_{var} = \begin{cases} 0, & \text{for } \alpha \leq 0.5 \\ \frac{1}{4} \sqrt{-1/\alpha^2 + 4}, & \text{for } \alpha > 0.5 \end{cases} \quad (5)$$

which indicates that the derivative of  $m_{var}$  is discontinuous at  $\alpha = 0.5$ , suggesting a disorder-order phase transition at  $\alpha_{c,var}$ . A comparison of  $m_{var}$  to the TRG result is given in Fig. 2(a), where  $m_{var}$  shows a behavior similar to the TRG results.

#### IV. GROUND-STATE PHASE DIAGRAM AND CRITICAL EXPONENTS IN PRESENCE OF A MAGNETIC FIELD

Now we turn the uniform magnetic field  $h$  on. The magnetization curves for different  $\alpha$  are given in Fig. 3. It is clear that for  $\alpha < \alpha_c$ , there exists a magnetization plateau with  $m_z = 0$ , where  $m_z = (1/N) \sum_i \langle S_i^z \rangle$  is the magnetization per site, implying the existence of a finite spin gap, as shown in Fig. 3(a) for  $\alpha = 0.3$ . At  $\alpha = 0$ , such a gap is nothing but the spin singlet-triplet gap which equals  $J$ . For  $0 < \alpha \leq \alpha_c$ , the spin gap will decrease and vanish eventually at  $\alpha = \alpha_c$ . For a given  $\alpha < \alpha_c$ , the spin gap closes at a critical field  $h_c$ . For  $h \gtrsim h_c$ , we find that the magnetization depends almost linearly on the magnetic field, behaving  $m_z \sim |h - h_c|^\beta$  with  $h_c = 0.604$ ,  $\beta = 0.98(1)$  for  $\alpha = 0.3$  and  $D = 5$ . Our result is consistent with the theoretical prediction  $\beta = 1.0$  in 2D

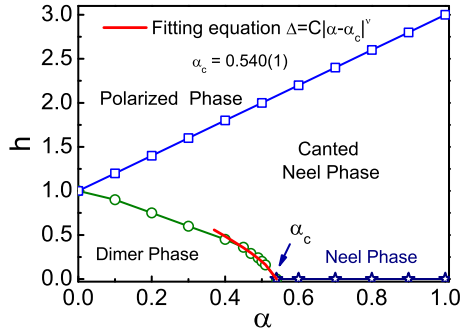


FIG. 4: (Color online) The ground state phase diagram of the spin-1/2 HAF system on the DHC lattice in  $\alpha$ - $h$  plane, where three phases (dimer, semiclassical Néel and polarized) are identified, and the collinear Néel phase marked by the star line inhabits exactly on the  $\alpha$  axis ( $h = 0$ ). The fitting curves reveal the critical behavior in the region  $\alpha \in [0.45, 0.51]$ .

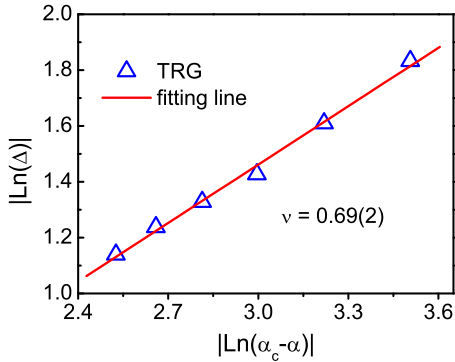


FIG. 5: (Color online) The log-log plot of spin gap  $\Delta$  versus  $\alpha$  in the critical region  $\alpha \in [0.45, 0.51]$ , where the linear fit gives the critical exponent  $\nu \simeq 0.69(2)$ .

and higher quantum spin systems<sup>6</sup>. Nonetheless, it is in sharp contrast to the cases of gapped one-dimensional Heisenberg spin systems where it is observed a square root dependence of  $m_z \sim |h - h_c|^{1/2}$  that characterizes the commensurate-incommensurate phase transition<sup>26</sup>. For other  $\alpha < \alpha_c$ , such an almost linear dependence was also noted. The susceptibility,  $\chi = \partial m_z / \partial h$ , as a function of the magnetic field  $h$  is shown in the upper inset of Fig. 3 (a). Two discontinuous points in  $\chi$  versus  $h$  are seen, namely one at the point  $h_c$  where the spin gap closes, and the other at the saturation field. We have also explored the transverse component of sublattice magnetization per site,  $m_{x,A} = \frac{1}{N_A} \sum_{i \in A} \langle S_i^x \rangle$ , against the magnetic field  $h$ , as given in the lower inset of Fig. 3(a). For  $\alpha < \alpha_c$ ,  $m_{x,A}$  vanishes for  $h \leq h_c$ , while it increases sharply when  $h$  exceeds  $h_c$ , and after reaching a round peak it declines steeply and vanishes at the saturation field. This observation shows that, with increasing the field, there exists a tran-

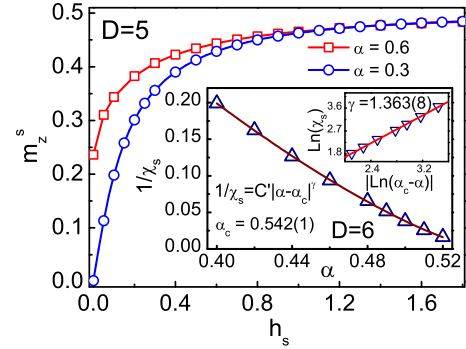


FIG. 6: (Color online) The staggered magnetization per site  $m_z^s$  as a function of the staggered magnetic field  $h_s$  for  $h = 0$ . The inset is  $1/\chi_s$  against  $\alpha$ , where the fitting curve is obtained at a small field  $h_s = 0.001J$ .

sition from the disordered dimer phase to a canted Néel phase (spin flop phase)<sup>4,5,22</sup> that is characterized by nonzero values of both  $m_z$  and  $m_{x,A}$ , where the spins align antiferromagnetically within the  $xy$  plane and develop a uniform  $z$  component along the field, thus canting out of the plane. For  $\alpha > \alpha_c$ , the magnetization curves behave differently from those with  $\alpha < \alpha_c$ , as presented in Fig. 3 (b) for  $\alpha = 0.8$  as an example. With increasing the magnetic field, the magnetization  $m_z$  increases monotonously till the saturation, while the transverse component of magnetization  $m_{x,A}$  first increases slowly, then drops sharply and vanishes eventually at the saturation field. The susceptibility  $\chi$  increases slowly with increasing the field, and then decreases steeply to zero at the saturation field.

By summarizing the above observations, a ground-state phase diagram of the system in the  $\alpha - h$  plane can be drawn, as presented in Fig. 4, where the phase boundaries are determined by the transition points in Figs. 2 and 3. One may see that there are three phases, namely, the dimer phase, the semiclassical Néel phase (including the canted and collinear Néel states) and the polarized phase. At  $\alpha = \alpha_c$ , there is a QPT from the disordered dimer phase to the collinear Néel phase. Note that the lower phase boundary between the dimer and canted Néel phases is determined by observing the spin gap  $\Delta$  that is obtained by calculating the width of zero magnetization plateau for various  $\alpha$  as presented in Fig. 3 (a). The critical behavior of the spin gap in the dimer phase in the vicinity of  $\alpha_c$  is fitted by the least squares method with  $\Delta \sim (\alpha - \alpha_c)^\nu$ , where  $\alpha_c \simeq 0.54$ , as shown in Fig. 4. The critical exponent is found to be  $\nu \simeq 0.69(2)$  by the linear fit, as shown in Fig. 5. It is close to the standard  $O(3)$  value of 0.7112(5) (e.g. Refs. 6,9,27). In comparison to the result  $\alpha_c = 0.27$  of the nonlinear  $\sigma$  model method<sup>28</sup> and the variational result  $\alpha_{c,var} = 0.5$  obtained through Eq. (3), the present TRG result is closer to  $\alpha_c = 0.576$  and  $\nu = 0.707$  of QMC calculations<sup>18</sup>. As expected, owing to its lower coordinates, the disordered region on the DHC lattice is wider than that on a square lattice where  $\alpha_c = 0.397^{10}$ .

In the presence of a staggered magnetic field  $h_s$ , the stag-

gered magnetization per site,  $m_z^s = (1/N) \sum_i \epsilon_i \langle S_i^z \rangle$ , as a function of  $h_s$  for different  $\alpha$  is presented in Fig. 6, where  $h = 0$ . With increasing  $h_s$ ,  $m_z^s$  increases monotonously from zero for  $\alpha < \alpha_c$ , while for  $\alpha > \alpha_c$ ,  $m_z^s$  starts from a nonzero value, implying again that the system has a spontaneous AFLRO for larger  $\alpha$ . The inverse of staggered susceptibility  $\chi_s = \partial m_z^s / \partial h_s$  as a function of  $\alpha$  is presented in the inset of Fig. 6 for  $h = 0$  and a very small  $h_s$ . The critical behavior of the zero-field staggered susceptibility  $\chi_s$  is expected to diverge as  $|\alpha - \alpha_c|^{-\gamma}$  near the critical point  $\alpha_c$ , where the nonlinear curve fitting gives  $\alpha_c \simeq 0.542(1)$  and the log-log plot in the inset shows the critical exponent  $\gamma \simeq 1.363(8)$ , which agree with  $\alpha_c$  obtained through the spin gap and the  $O(3)$  value of  $\gamma = 1.373(3)$ <sup>27</sup>, respectively. According to the obtained critical exponents  $\beta$  and  $\gamma$ , it is seen that the quantum criticality of the present system falls into the  $O(3)$  universality class. Similar calculations indicate that the transition between the dimer and canted Néel phases have the same critical exponents  $\beta$  and  $\gamma$  as that of the dimer-collinear Néel phase transition at  $h = 0$ . Hence, they also belong to the same  $O(3)$  universality class.

## V. RELATION TO THE 2D BOSON HUBBARD MODEL

Finally, we would like to mention briefly that the present spin-1/2 system has a link with the 2D boson Hubbard model. By performing the hard-core boson mapping<sup>29</sup> with  $a_i^\dagger \rightarrow S_i^+$ ,  $a_i \rightarrow S_i^-$ ,  $n_i \rightarrow S_i^z + 1/2$ , and making a rotation of spins by  $\pi$  along the  $z$  axis on one sublattice, one can obtain, from Eq. (1) with  $h_s = 0$ , the Hamiltonian of hard-core bosons

$$\begin{aligned}
 H_b = & \sum_{\langle i,j \rangle_x} [-t(a_i^\dagger a_j + a_j^\dagger a_i) + U(n_i - 1/2)(n_j - 1/2)] \\
 & + \sum_{\langle i,j \rangle_{yz}} [-t'(a_i^\dagger a_j + a_j^\dagger a_i) + U'(n_i - 1/2)(n_j - 1/2)] \\
 & - \mu \sum_i (n_i - 1/2), \quad (6)
 \end{aligned}$$

where  $t = U = J$ ,  $t' = U' = J'$  and  $\mu = h$ . It is the boson Hubbard model on the DHC lattice, whose behavior can be well understood in accordance with the aforementioned cor-

responding Heisenberg spin system. With the above mapping, owing to the nonvanishing sublattice magnetization  $|m_{x,A(B)}|$  in  $x$ - $y$  plane (see the inset of Fig. 3), the canted Néel phase in the spin system corresponds to the boson superfluid phase with off diagonal long-range order (ODLRO)<sup>22,30</sup> in the boson Hubbard model for  $t'/t = U'/U > 0.54$  on the DHC lattice. For  $t'/t = U'/U < 0.54$ , the disordered dimer phase in the spin system is mapped onto a liquid state with neither ODLRO nor DLRO. Therefore, the boson Hubbard model on the DHC lattice has a QPT from the boson liquid to a superfluid. The spin polarized phase becomes a Mott insulator phase with one boson occupying each site in the mapped boson system, and hence, there also exists a superfluid-Mott insulator transition.

## VI. CONCLUSION

In conclusion, the spin-1/2 HAF model on the DHC lattice is studied by means of the combined iTEBD and TRG algorithm, where the ground-state phase diagram is obtained. It is uncovered that there is a second-order QPT from the disordered dimer phase to the ordered collinear Néel phase at  $\alpha_c \simeq 0.54$ , where the critical exponents  $\nu \simeq 0.69(2)$  and  $\gamma \simeq 1.363(8)$  are determined. This QPT belongs to the standard  $O(3)$  universality class. In addition, through a boson mapping, the present HAF system has a link with the boson Hubbard model on the DHC lattice. The properties of the latter boson Hubbard model can thus be understood in terms of the present study. We expect that our findings is not only useful for understanding experimental observations of the antiferromagnets with DHC lattices, but also is helpful for the corresponding 2D boson Hubbard model.

## Acknowledgments

The authors are grateful to H. C. Jiang, Z. Y. Xie, and T. Xiang for stimulating discussions. We are also indebted to Z. Y. Chen, Y. T. Hu, Z. C. Wang, Q. B. Yan, F. Ye, and Q. R. Zheng for useful discussions. This work is supported in part by the NSFC (Grant Nos. 10625419, 10934008, 90922033), the MOST of China (Grant No. 2006CB601102) and the Chinese Academy of Sciences.

<sup>1</sup> \*Corresponding author. Email: gsu@gucas.ac.cn

<sup>2</sup> J.D. Reger, J.A. Riera and A.P. Young, J. Phys. Condens. Matter **1**, 1855 (1989).

<sup>3</sup> Zheng Weihong, J. Oitmaa, and C.J. Hamer, Phys. Rev. B **43**, 8321 (1991).

<sup>4</sup> M. E. Zhitomirsky and T. Nikuni, Phys. Rev. B **57**, 5013 (1998).

<sup>5</sup> A. Lüscher and A. M. Läuchli, Phys. Rev. B **79**, 195102 (2009).

<sup>6</sup> S. Sachdev, *Quantum Phase Transition* (Cambridge University Press, Cambridge, 1999); Nat. Phys. **4**, 173 (2008).

<sup>7</sup> S.E. Krüger, J. Richter, J. Schülenburg, D.J.J. Farnell, and R.F. Bishop, Phys. Rev. B **61**, 14607 (2000).

<sup>8</sup> R.R.P. Singh, M.P. Gelfand, and D.A. Huse, Phys. Rev. Lett. **61**,

2484 (1988).

<sup>9</sup> M. Matsumoto, C. Yasuda, S. Todo, and H. Takayama, Phys. Rev. B **65**, 014407 (2001).

<sup>10</sup> S. Wenzel, L. Bogacz, and W. Janke, Phys. Rev. Lett. **101** 127202 (2008); S. Wenzel and W. Janke, Phys. Rev. B **79** 014410 (2009).

<sup>11</sup> J. Oitmaa, C. J. Hamer, and Zheng Weihong, Phys. Rev. B **45**, 9834 (1992).

<sup>12</sup> Zheng Weihong, J. Oitmaa, and C.J. Hamer, Phys. Rev. B **44**, 11869 (1991).

<sup>13</sup> H.C. Jiang, Z.Y. Weng, and T. Xiang, Phys. Rev. Lett. **101** 090603 (2008); Z.Y. Xie, H.C. Jiang, Q.N. Chen, Z.Y. Weng, and T. Xiang, Phys. Rev. Lett. **103**, 160601 (2009).

- <sup>14</sup> P. A. Joy and S. Vasudevan, Phys. Rev. B **46**, 5425 (1992).
- <sup>15</sup> V. Kataev, A. Müller, U. Löw, W. Jung, N. Schittner, M. Kriener, A. Freimuth, J. Magn. Mater. **290-291**, 310 (2005).
- <sup>16</sup> Y. Miura, R. Hirai, Y. Kobayashi, and M. Sato, J. Phys. Soc. Jpn. **75**, 084707 (2006).
- <sup>17</sup> I. Spremo, F. Schütz, P. Kopietz, V. Pashchenko, B. Wolf, M. Lang, J. W. Bats, C. Hu, and M. U. Schmidt, Phys. Rev. B **72**, 174429 (2005).
- <sup>18</sup> F.-J. Jiang, U. Gerber, arXiv:0906.2539v3 (2009).
- <sup>19</sup> M. Levin and C. P. Nave, Phys. Rev. Lett. **99**, 120601 (2007).
- <sup>20</sup> Z. C. Gu, M. Levin, and X. G. Wen, Phys. Rev. B **78**, 205116 (2008).
- <sup>21</sup> G. Vidal, Phys. Rev. Lett. **98**, 070201 (2007); R. Orús and G. Vidal, Phys. Rev. B **78**, 155117 (2008).
- <sup>22</sup> P. Chen, C.Y. Lai, and M.F. Yang, J. Stat. Mech. P10001 (2009).
- <sup>23</sup> U. Löw, Condensed Matter Physics **12**, 497 (2009).
- <sup>24</sup> H.H. Zhao, Z. Y. Xie, Q. N. Chen, Z.C. Wei, J.W. Cai, and T. Xiang, arXiv:1002.1405v1 (2010).
- <sup>25</sup> C. Gros, W. Wenzel, and J. Richter, Europhys. Lett. **32**, 747 (1994).
- <sup>26</sup> R. Chitra and T. Giamarchi, Phys. Rev. B **55**, 5816 (1997).
- <sup>27</sup> K. Chen, A. M. Ferrenberg, and D. P. Landau, Phys. Rev. B **48**, 3249 (1993); M. Campostrini, M. Hasenbusch, A. Pelissetto, P. Rossi, and E. Vicari, Phys. Rev. B **65**, 144520 (2002).
- <sup>28</sup> K. Takano, Phys. Rev. B **74**, 140402(R) (2006).
- <sup>29</sup> T. Matsubara and H. Matsuda, Prog. Theor. Phys. **16**, 569 (1956).
- <sup>30</sup> S. Wessel, Phys. Rev. B **75**, 174301 (2007); J.Y. Gan, Y.C. Wen, J. Ye, T. Li, S.J. Yang, and Y. Yu, *ibid* **75**, 214509 (2007).